Nano Research

Open Access

Research Article

Copper phosphide coupled with amorphous ruthenium on scaffold surfaces synergistically enhances hydrogen production

Miaoyang Yu[1,3,§], Qiao Ye[1,§], Linfeng Xiao[2], Xiaojun Zeng[2] ✉, Feng Wang[1,3], Abdukader Abdukayum[3], Chuan Zuo[4] ✉, Weiping Liu[4], Nianpeng Li[5], Guangzhi Hu[5], and Xue Zhao[1] ✉

[1] *Yunnan Key Laboratory of Modern Separation Analysis and Substance Transformation, College of Chemistry and Chemical Engineering, Yunnan Normal University, Kunming 650500, China*
[2] *Jiangxi Key Laboratory of Advanced Ceramic Materials, School of Materials Science and Engineering, Jingdezhen Ceramic University, Jingdezhen 333403, China*
[3] *Xinjiang Key Laboratory of Novel Functional Materials Chemistry, College of Chemistry and Environmental Sciences, Kashi University, Kashi 844000, China*
[4] *Yunnan Precious Metals Laboratory, Guiyan Chemical Materials Co., Ltd., Kunming 650106, China*
[5] *Institute for Ecological Research and Pollution Control of Plateau Lakes, School of Ecology and Environmental Science, Yunnan University, Kunming 650500, China*
[§] *Miaoyang Yu and Qiao Ye contributed equally to this work.*

Cite this article: *Nano Research*, **2026**, *19*, 94908527. https://doi.org/10.26599/NR.2026.94908527

ABSTRACT: Water electrolysis is an ideal way to obtain "green hydrogen", but the core challenge of its commercial application is to develop advanced electrocatalysts that can work efficiently and stably under wide pH conditions. In this study, we innovatively constructed a Cu_3P support with a unique pyramid-like crystal structure by controllable surface oxidation and phosphating treatment on the three-dimensional (3D) copper foam skeleton, and further loaded ruthenium (Ru) to form a Ru-Cu_3P/CF self-supporting electrode to form a unique composite structure. Ampere-grade hydrogen evolution at full pH was achieved. Benefiting from the fast charge transport guaranteed by the 3D conductive network, and the electronic synergistic effect between Ru and Cu_3P support. the as-prepared Ru-Cu_3P/CF catalyst enables better catalytic performance than commercial Pt/C catalyst in the whole pH range. Under alkaline and acidic conditions, the overpotential required to drive hydrogen evolution reaction (HER) to current density of 1 A·cm^{-2} is only 241.7 and 281.3 mV. At the same time, under the working condition, Ru-Cu_3P/CF also inherits excellent HER performance, which realizes the efficient electrolysis of seawater to produce hydrogen and the ampere-grade hydrogen evolution at low voltage (1.79 V) on the integrated membrane electrode assembly. The performance of Ru-Cu_3P/CF catalyst is significantly better than that of most reported Ru-based catalysts. This work provides a new idea for the design of integrated electrocatalysts with high performance and low noble metal loading.

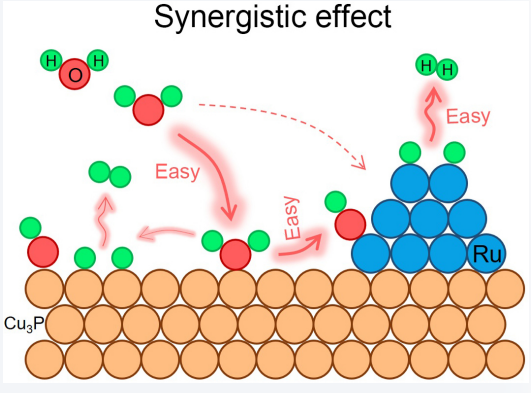

KEYWORDS: water electrolysis, hydrogen evolution, synergistic catalysis, ruthenium, seawater

1 Introduction

Hydrogen production from electrolyzed water is the key to the development of green hydrogen energy economy [1–6]. The core of its industrial application is to develop an all-pH hydrogen evolution reaction (HER) catalyst that can operate continuously and stably at ampere-level current density [7–9]. Although precious metal catalysts show excellent performance at high current densities, their high cost and natural scarcity severely limit large-scale applications [10–12]. Therefore, developing new catalytic systems that are suitable for ampere-level current densities, with significantly reduced precious metal loading while maintaining high activity and stability, constitutes a major challenge in the current field [13–18].

Coupling with high-yield non-precious metals to build synergistic effects is an effective strategy for optimizing HER

Received: November 19, 2025; **Revised:** January 2, 2026
Accepted: February 3, 2026

✉Address correspondence to Xue Zhao, zhaoxue@ynnu.edu.cn; Xiaojun Zeng, zengxiaojun@jcu.edu.cn; Chuan Zuo, zuochuan@ipm.com.cn

catalysts [19–24]. Among them, copper exhibits catalytic potential due to the flexible electronic structure endowed by its various oxidation states ($Cu^0/Cu^+/Cu^{2+}$). Its three-dimensional (3D) structure can promote electrolyte mass transfer and bubble desorption, which is expected to achieve efficient and stable catalysis at high current density [25–27]. Copper foam has been widely studied as a catalyst carrier in the field of electrocatalytic hydrogen evolution due to its high specific surface area, excellent conductivity and low cost. For example, Shen et al. constructed a ruthenium (Ru)-doped 3D cuprous oxide nanochain, showing excellent HER and hydrazine oxidation reaction (HzOR) performance, but still did not achieve efficient hydrogen evolution of the catalyst at an ampere-grade current density [28]. Xi et al. used a one-step hydrolysis method to synthesize Cu-doped RuO_2 (Cu-RuO_2), and the constructed Ru^0/Ru^{4+} double sites significantly improved the alkaline HER performance [29]. However, the preparation process is complicated, and the reduction of RuO_2 to Ru requires high energy, which is difficult to achieve large-scale application. Copper foam, due to its three-dimensional porous structure and excellent conductivity, has become one of the ideal candidate materials for HER catalyst carriers. However, its industrial application faces a key challenge: While the three-dimensional porous structure provides high specific surface area and mass transfer efficiency, it is often accompanied by relatively insufficient electrochemical stability, and the contradiction between these two needs to be addressed urgently [30]. Under the working conditions of HER, the interface of copper foam is prone to corrosion, resulting in catalyst shedding and performance degradation. Although the existing surface modification technology can improve the stability, it is often difficult to balance the protection effect and process feasibility-the preparation of high-efficiency coatings is complex and difficult to scale up, and the simple method cannot guarantee the uniformity and durability.

In view of the above problems, a Ru-doped copper phosphide (Ru-Cu_3P/CF) composite catalyst based on 3D copper foam (CF) was designed and successfully prepared. In this design, Cu_3P with a pyramid-like crystal structure was *in-situ* grown on the surface of CF skeleton by a continuous process of oxidation followed by phosphating. This unique microstructure not only provides a huge specific surface area, but its pyramid shape itself also helps to induce a local high electric field at ampere-level current density, thereby promoting proton adsorption and conversion. On this basis, trace Ru was further loaded by mild chemical deposition to form uniformly distributed spherical aggregates, and finally Ru-Cu_3P/CF heterostructure was constructed. The electrochemical tests of the system show that the composite catalyst exhibits excellent HER performance in acidic, alkaline and neutral electrolytes, and can operate stably at an ampere-level current density of more than 1 $A{\cdot}cm^{-2}$, achieving efficient hydrogen evolution under full pH conditions.

2 Materials fabrication

First, the copper foam (2 cm × 3 cm) was ultrasonically cleaned sequentially in 3 M HCl, deionized water, and ethanol for 30 min, and then dried in an oven at 60 °C for 6 h. The treated copper foam was immersed into a 3 M NaOH solution, and oxygen was introduced into the solution until it turns blue. Then the system was placed in a 40 °C water bath, and 1 mL of H_2O_2 was added dropwise to the solution until the blue solution became transparent. The copper foam was removed, washed multiple times with ethanol, and dried at 60 °C for 12 h to obtain Cu_2O/CF. The obtained Cu_2O/CF was placed downstream of a tubular furnace, with phosphorus powder upstream, and calcined under a N_2 atmosphere. The program was heated to 350 °C (heating rate 5 $°C{\cdot}min^{-1}$) and maintained for 2 h to obtain Cu_3P/CF. Cu_3P/CF (2 cm × 2 cm) was taken and immersed in solution A (prepared by dissolving 0.93 g KCl and 0.1 mmol $RuCl_3$ in 50 mL deionized water), and electrodeposition was performed in a conventional three-electrode system (constant potential −1.66 V, deposition time 900 s). After washing and drying, Ru-Cu_3P/CF was obtained. As a control, Cu_3P/CF was obtained under the same subsequent treatment without the oxidation step, referred to as Cu_3Posp/CF.

Other experimental details were placed in the Eletronic Supplementary Material (ESM).

3 Results and discussion

Using CF as the substrate, Cu_3P with a pyramid-like crystal structure was obtained by surface oxidation-phosphating treatment, and then Ru-Cu_3P/CF composite catalyst composed of spherical aggregates was successfully prepared by loading Ru. X-ray diffraction (XRD) phase analysis showed that the copper foam substrate produced a strong diffraction background signal, while the characteristic diffraction signal of the loaded ruthenium was extremely weak due to its low content and high dispersion. Therefore, the strong background signal completely obscures the weak Ru characteristic peak, making it impossible to be observed in the XRD pattern (Fig. S1 in the ESM).

X-ray photoelectron spectroscopy (XPS) analysis confirmed that although Ru is mainly zero-valent, there is still a small amount of oxidation state, which is attributed to the inevitable oxidation of its surface (Fig. S2 in the ESM). In addition, the valence state of the metal did not change before and after Ru-Cu_3P/CF catalyzed HER (Fig. S3 in the ESM). Scanning electron microscopy (SEM) analysis shows that the morphology evolution of the material presents a clear multi-level structure, the pretreated CF provides anchoring sites for subsequent growth through surface cracking; after oxidation-phosphorization, it is converted into a pyramid-like crystal structure Cu_3P (Figs. S4–S6 in the ESM); finally, Ru was electrodeposited on Cu_3P to form spherical aggregates as active centers (Fig. 1(a)).

In addition, SEM results reveal the key role of oxidation treatment on the morphology of the final material. In the control experiment of omitting the oxidation step, the Cu_3Posp/CF (one step phosphating) obtained by direct phosphating showed a relatively flat irregular block morphology (Fig. S7 in the ESM). In stark contrast, the material treated by oxidation-phosphating two-step treatment exhibits a rich three-dimensional rough structure. This proves that the oxidation process can effectively reconstruct the microstructure of the copper foam precursor. This reconstructed structure is retained after phosphating, and finally provides an ideal carrier for the uniform deposition and high dispersion of ruthenium (Fig. S8 in the ESM). In addition, after catalyzing HER, the morphology changes slightly. This evolution is usually directly related to the exposure of active sites or the increase of surface roughness, which is intuitive evidence that the material is activated during the reaction (Fig. S9 in the ESM). Transmission electron microscopy (TEM) analysis shows that the material exhibits a clear Cu_3P pyramid morphology (Fig. 1(b)). High-

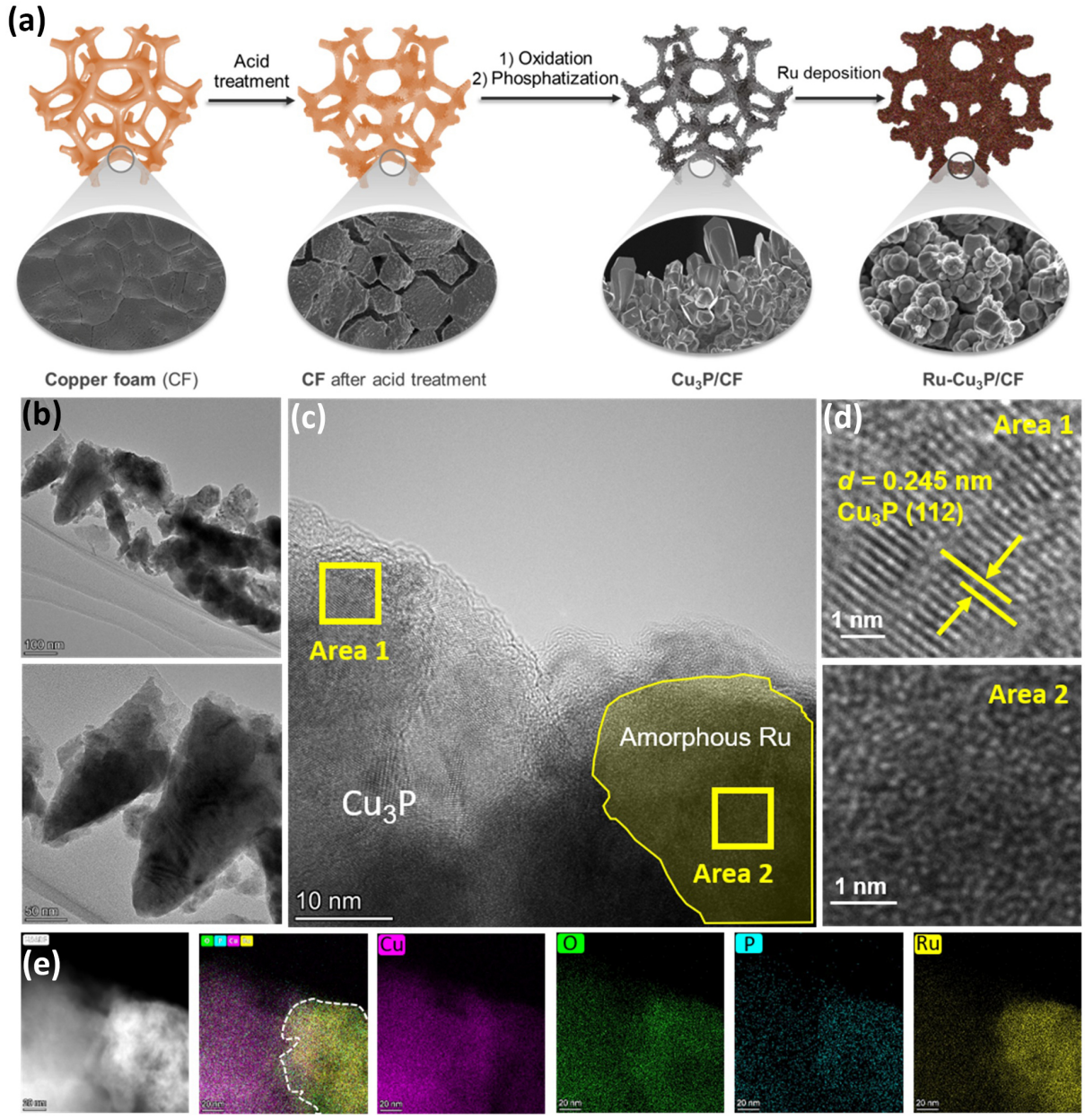

Figure 1 (a) Preparation process diagram of Ru-Cu_3P/CF. (b) SEM images of Ru-Cu_3P/CF. (c) and (d) HRTEM images and lattice spacing of Ru and Cu_3P in Ru-Cu_3P/CF. (e) Element distribution in Ru-Cu_3P/CF.

resolution TEM (HRTEM) shows that the lattice fringe spacing is 0.245 nm (Fig. S10 in the ESM), which belongs to the (112) crystal plane of Cu_3P, while Ru exists in an amorphous state (Figs. 1(c) and 1(d)). Element mapping further confirmed that the Ru element signal overlapped and adjacent to the Cu and P signal regions, forming an obvious interface boundary, indicating that Ru had been successfully anchored on the surface of the Cu_3P support (Fig. 1(e) and Fig. S11 in the ESM). In addition, it also corresponds to energy dispersive X-ray spectroscopy (EDX) and atomic percentage statistical table (Fig. S12 and Tables S1 and S2 in the ESM).

To systematically evaluate the catalytic performance of Ru-Cu_3P/CF for HER, the catalytic performance of Ru-Cu_3P/CF for HER was evaluated in alkaline (1.0 M KOH solution), acidic (0.5 M H_2SO_4 solution), and neutral (1.0 M PBS solution) electrolytes, respectively. From the linear sweep voltammetry curve (LSV), it can be seen that in alkaline and acidic electrolytes, the current density of HER driven by Ru-Cu_3P/CF to reach 1 $A \cdot cm^{-2}$ only requires an overpotential of 241.70 and 281.30 mV, which is significantly better than its commercial Pt/C and other comparison samples (Figs. 2(a) and 2(b), and Figs. S13 and S14 in the ESM). In neutral electrolyte, the current density of Ru-Cu_3P/CF-driven HER reaches 10 $mA \cdot cm^{-2}$ with only an overpotential of 291.30 mV (Fig. 2(c)). At the same time, the performance of Ru-Cu_3P/CF catalyst for HER is better than most of the catalysts reported in the literature (Figs. S15–S17 and Tables S3–S5 in the ESM). In addition, in alkaline, acidic, and neutral electrolytes, Tafel is also as low as 16.80, 3.37, and 6.21 $mV \cdot dec^{-1}$, respectively (Figs. 2(d)–2(f)). The above results show that Ru-Cu_3P/CF has good HER catalytic performance in a wide pH range. The durability of catalysts is crucial in industrial applications. In this work, the stability of Ru-Cu_3P/CF in catalyzing

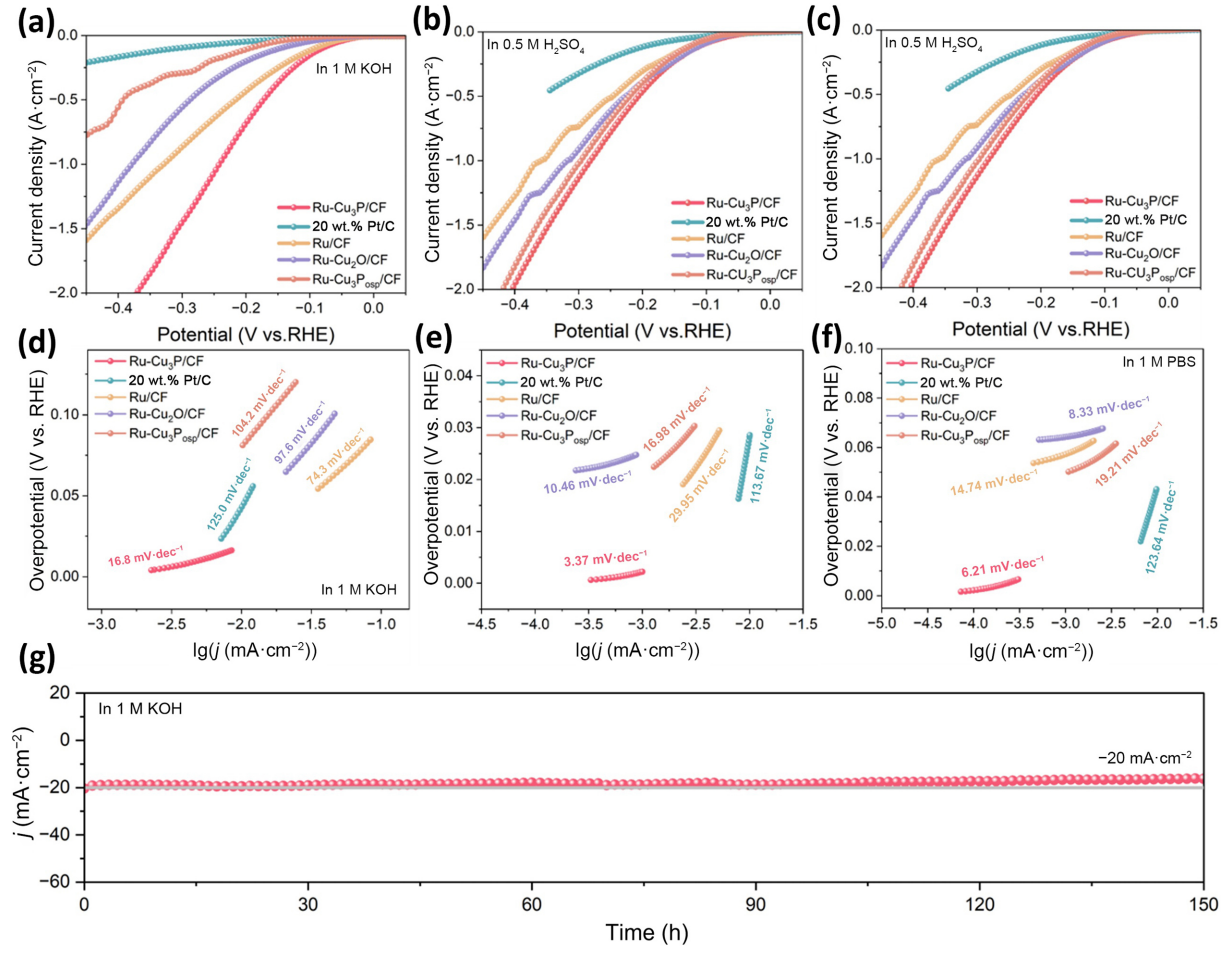

Figure 2 Evaluation of HER performance of different catalysts. (a)–(c) LSV polarization curves in alkaline, acidic, and neutral, respectively. (d)–(f) The Tafel slopes in alkaline, acidic, and neutral, respectively. (g) Stability in 1 M KOH electrolyte (at a current density of –20 mA·cm^{-2}).

HER in alkaline, acidic and neutral media was studied by accelerated cyclic voltammetry. After running accelerated cyclic voltammetry for 10,000 times, the current density of the catalytic HER in alkaline, acidic, and neutral was slightly attenuated (LSV curve), but the overpotential at a current density of 1 A·cm^{-2} was only attenuated by 7, 5, and 4 mV, respectively (Fig. S18 in the ESM). In addition, Ru-Cu_3P/CF continuously catalyzes HER for 150 h in alkaline electrolyte, and the current density does not fluctuate significantly (Fig. 2(g)). Therefore, Ru-Cu_3P/CF have good electrochemical stability in catalyzing HER. The results of electrochemical impedance spectroscopy showed that the Ru-Cu_3P/CF catalyst had the smallest charge transfer resistance compared with Ru-Cu_2O/CF, Ru-Cu_3P_{osp}/CF and Ru/CF catalysts, which proved its faster interface electron transport rate (Fig. S19 in the EMS).

In addition, the electrochemical active area was evaluated by double layer capacitance test. The C_{dl} value of Ru-Cu_3P/CF was as high as 29.51 mF·cm^{-2}, which was higher than that of other contrast samples, indicating that it had a larger active surface area (Fig. S20 in the ESM). These results together indicate that the excellent HER performance of Ru-Cu_3P/CF is due to the synergistic effect of its enhanced charge transfer kinetics and significantly increased exposure rate of active sites.

To evaluate the electrocatalytic hydrogen evolution reaction performance of Ru-Cu_3P/CF in complex real environment [31–34], we systematically tested the polarization curves of Ru-Cu_3P/CF in seawater, alkaline seawater (1 M KOH) and simulated seawater (1 M KOH + 0.5 M NaCl). The LSV test results show that the HER activity of Ru-Cu_3P/CF is significantly better than that of commercial Pt/C catalyst in all the above media (Figs. 3(a) and 3(b), and Figs. S21 and S22 in the ESM). This finding confirms that Ru-Cu_3P/CF has the potential to efficiently drive hydrogen evolution reaction in a variety of seawater matrices, showing its superiority in practical applications. In order to achieve large-scale hydrogen production, stack catalysts must withstand significant fluctuations in electrolyte temperature caused by environmental and operating conditions [35]. The performance evaluation confirmed that Ru-Cu_3P/CF can maintain high activity and stability in a wide temperature range of 5–60 °C across electrolyte (acid, alkali, and neutral) with different pH values, and its Ru-Cu_3P/CF synthesis catalytic performance surpasses the commercial Pt/C catalyst (Figs. S23–S25 in the ESM).

In order to evaluate the application potential in the actual alkaline water electrolysis device, we assembled a film-forming electrode (MEA) with Ru-Cu_3P/CF as cathode and RuO_2 anode for testing [36, 37]. The performance test results show that when the current density reaches 1 A·cm^{-2}, the cell voltage is only 1.79 V, which is significantly better than the commercial Pt/C catalyst tested under the same conditions. The above results confirm the excellent electrocatalytic performance of Ru-Cu_3P/CF at high current density, highlighting its practical application prospects in high-power water electrolysis hydrogen production stacks (Figs. 3(c) and 3(d)).

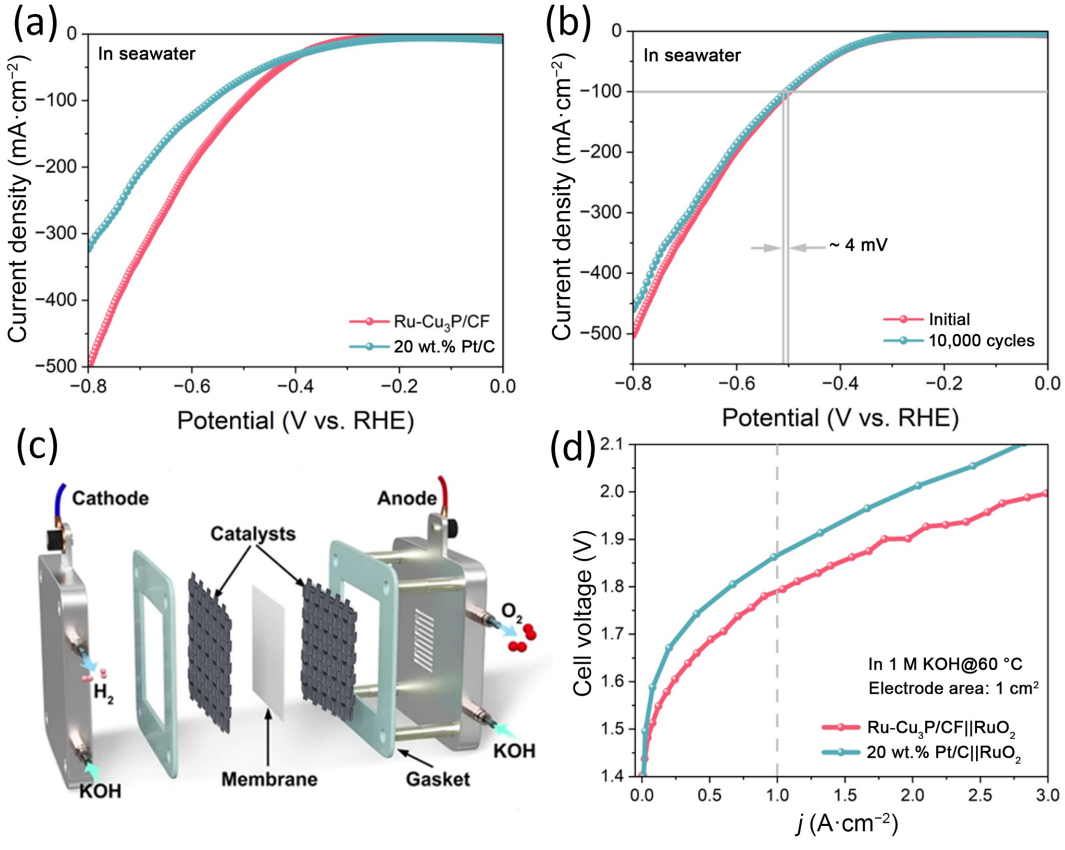

Figure 3 (a) Seawater electrolysis system with Ru-Cu_3P/CF or 20 wt.% Pt/C as a catalyst. (b) The LSV curves of Ru-Cu_3P/CF as a catalyst were collected in seawater. (c) Membrane electrode schematic diagram. (d) LSV polarization curves of Ru-Cu_3P/CF and 20 wt.% Pt/C in membrane electrode.

To further explore the HER reaction mechanism of Ru-Cu_3P/CF, we used *in-situ* electrochemical attenuated total reflection Fourier transform infrared spectroscopy to monitor the electrode/solution interface in real time [38, 39] (Fig. 4(a)). The dynamic changes of spectra reveal that the signals of O–H stretching vibration (~ 3400 cm^{-1}) and H–O–H bending vibration (~ 1600 cm^{-1}) of interfacial water molecules are simultaneously enhanced with the continuous negative shift of the applied reduction potential, which intuitively reflects the interfacial water. The reorganization of the molecular structure and the increase of the density of water molecules mean that the electrode surface forms a local microenvironment that is more conducive to triggering the water decomposition reaction. More importantly, we clearly detected the characteristic vibration signal of the Ru–H bond, and its intensity increased with the negative shift of the potential, which provided direct spectral evidence for the dissociation of water molecules at the Ru site and the formation of adsorbed hydrogen intermediates, and clarified the smooth progress of this step in the catalytic cycle (Figs. 4(b)–4(d)).

In addition, *in-situ* Raman spectroscopy revealed that under electrocatalytic conditions, the water molecules at the catalyst/electrolyte interface were not disorderly distributed, but spontaneously assembled to form three structured networks with clear characteristics, K-hydrate clusters, two-dimensional double hydrogen bond interface network and three-dimensional four hydrogen bond body phase network [40, 41]. This highly ordered interfacial water molecular layer significantly improves the performance of electrolytic water through multiple synergistic mechanisms (Fig. 4(e)).

Based on density functional theory (DFT) calculations, the catalytic models of Cu_3P, Ru, and Ru-Cu_3P/CF were systematically constructed in this study (Figs. 5(a)–5(c)), and the HER performance differences of different metal sites were analyzed in depth. In Cu_3P, due to the high electronegativity of P atom, there is a significant charge polarization between P atom and Cu atom. When Cu_3P contacts with Ru with higher work function to form a heterogeneous interface, in order to achieve the balance of Fermi level, electrons will spontaneously transfer from Cu_3P to Ru side (Fig. 5(d)). The Gibbs free energy calculation (Fig. 5(e)) shows that the Ru-Cu_3P site is easier to desorb [H] to form H_2 than the Ru site and the Cu_3P site under acidic conditions. In alkaline and neutral media, the content of H^+ is low and depends on the adsorption and dissociation of water. DFT calculations show that compared with Ru-Cu_3P sites, Ru sites and Cu_3P sites have the lowest adsorption energy for water molecules (Fig. 5(f)), which is more conducive to the capture of water. At the same time, the dissociation of water molecules is also important. The dissociation energy of H_2O at Ru-Cu_3P is significantly lower than that of H_2O at Ru or Cu_3P sites (Fig. 5(g)). These calculations reveal that the heterogeneous interface formed by Ru and Cu_3P optimizes the electronic structure of the active site through spontaneous electron transfer, which effectively regulates the adsorption strength of the [H], thereby improving the intrinsic reactivity. Among them, Ru-Cu_3P is advantageous in adsorbing protons (H^+) to promote acidic HER, while Ru and Cu_3P are beneficial to capture water molecules (H_2O) to enhance alkaline and neutral HER. These two cooperate and couple with the copper foam substrate to ensure the rapid reaction kinetics and excellent stability in the whole pH range (Fig. 5(h) and Fig. S26 in the ESM).

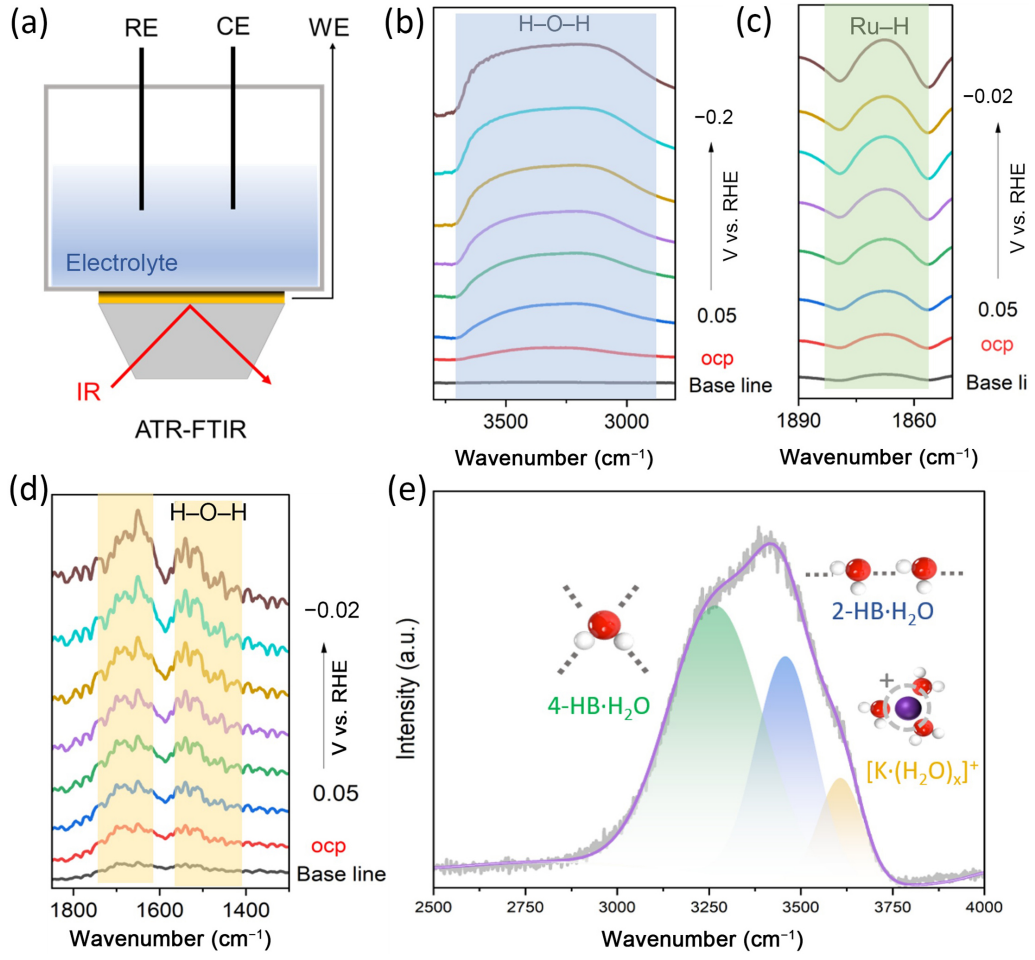

Figure 4 (a) *In-situ* electrochemical ATR-FTIR test principle. (b)–(d) *In-situ* electrochemical ATR-FTIR signal of HER catalyzed by Ru-Cu_3P/CF. (e) Aggregation behavior of water molecules at the interface of Ru-Cu_3P/CF catalyst.

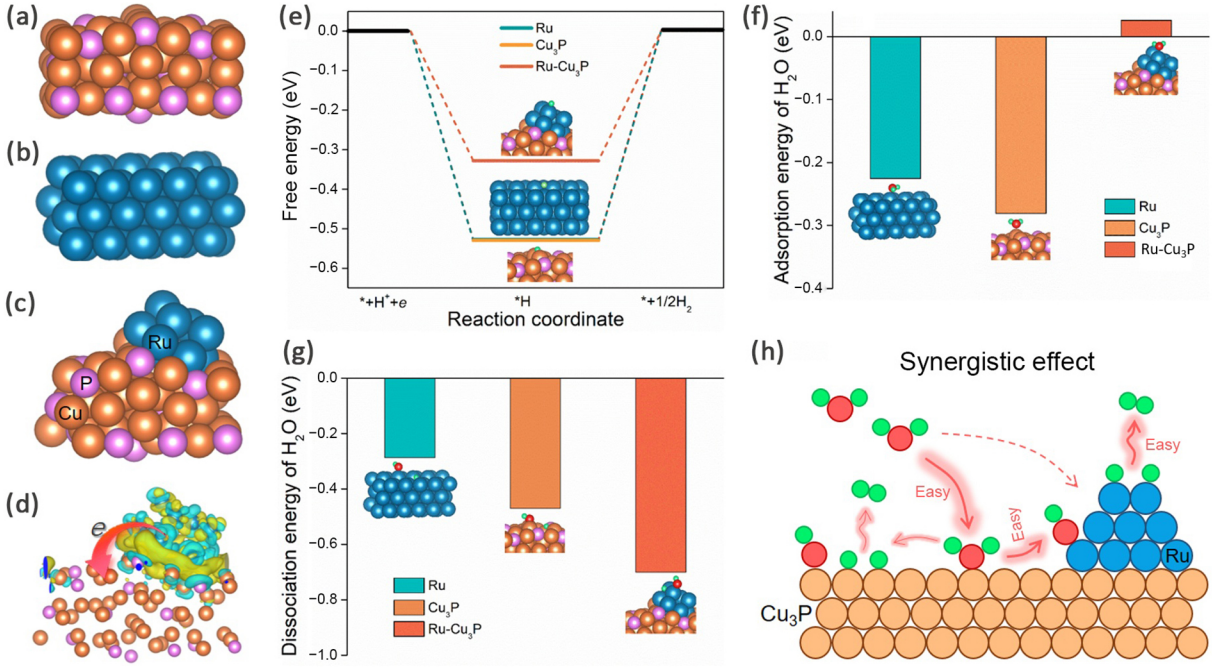

Figure 5 (a)–(c) The atomic model diagrams of Cu_3P, Ru, and Ru-Cu_3P/CF. (d) A schematic diagram of electron transfer from Cu_3P to Ru. (e) The adsorption free energy of *H on the active sites of Ru, Cu_3P, and Ru-Cu_3P/CF. (f) Adsorption energy and (g) desorption energy of water on the active sites of Ru, Cu_3P, and Ru-Cu_3P/CF. (h) A schematic diagram of the capture and dissociation of water molecules at the Ru-Cu_3P/CF interface.

4 Conclusion

In this study, a Ru-based composite catalyst (Ru-Cu_3P/CF) with pyramid-like Cu_3P as support was constructed *in situ* on copper foam by a controllable surface engineering strategy. The design aims to simultaneously optimize charge transport and active site exposure, so that it exhibits hydrogen evolution activity and stability beyond commercial Pt/C in a wide pH environment including seawater (150 h decay < 5 %). In alkaline and acidic electrolytes, the overpotentials of Ru-Cu_3P/CF-driven HER are as low as 241.7 and 281.3mV at a current density of 1 A·cm^{-2}, respectively. In addition, in neutral electrolyte, the overpotential of Ru-Cu_3P/CF-driven HER is as low as 105.1 mV at a current density of 100 mA·cm^{-2}, which is better than that of commercial Pt/C catalyst. This work not only confirms the practical application potential of Ru-Cu_3P/CF, but also provides an innovative material design idea for the design of high-performance and corrosion-resistant catalysts for complex electrolytic environments.

Electronic Supplementary Material: Supplementary material (material characterization method, electrochemical test, *in-situ* attenuated total reflection Fourier transform infrared, Figs. S1–S26, Table S1–S5, and supplementary references) is available in the online version of this article at https://doi.org/10.26599/NR.2026.94908527.

Data availability

All data needed to support the conclusions in the paper are presented in the manuscript and the Electronic Supplementary Material. Additional data related to this paper may be requested from the corresponding author upon request.

Acknowledgements

The authors thank for the financial support from the Xingdian Talent Program of Yunnan Province (2023), Yunnan Fundamental Research Projects (Nos. 202401CF070026 and 202501AT070017), the Scientific Research Fund Project of Yunnan Provincial Education Department (No. 2024J0134), and the Scientific and Technological Project of Yunnan Precious Metals Laboratory (No. YPML-20240502065).

Declaration of competing interest

All the contributing authors report no conflict of interests in this work.

Author contribution statement

M. Y. Y.: Investigation, writing – original draft, visualization. Q. Y.: Investigation, writing – original draft, validation. L. F. X.: Investigation, writing – review & editing. X. J. Z.: Project administration, writing – review & editing, supervision, resources, formal analysis. F. W.: Writing – review & editing. A. A.: Writing – review & editing, supervision. C. Z.: Writing – review & editing, supervision. W. P. L.: Writing – review & editing, supervision. N. P. L.: Writing – review & editing. G. Z. H.: Conceptualization, supervision, funding acquisition. X. Z.: Conceptualization, supervision, software, formal analysis, investigation, resources, writing – review & editing, visualization, project administration, funding acquisition.

Use of AI statement

None.

References

[1] Qian, Q. Z.; Zhu, Y.; Ahmad, N.; Feng, Y. F.; Zhang, H. K.; Cheng, M. Y.; Liu, H. H.; Xiao, C.; Zhang, G. Q.; Xie, Y. Recent advancements in electrochemical hydrogen production via hybrid water splitting. *Adv. Mater.* **2024**, *36*, 2306108.

[2] Vilanova, A.; Dias, P.; Lopes, T.; Mendes, A. The route for commercial photoelectrochemical water splitting: A review of large-area devices and key upscaling challenges. *Chem. Soc. Rev.* **2024**, *53*, 2388–2434.

[3] Boettcher, S. W. Introduction to green hydrogen. *Chem. Rev.* **2024**, *124*, 13095–13098.

[4] Neumann, F.; Zeyen, E.; Victoria, M.; Brown, T. The potential role of a hydrogen network in Europe. *Joule* **2023**, *7*, 1793–1817.

[5] Feng, C. Y.; Raziq, F.; Huang, H. W.; Wu, Z. P.; Alqahtani, H. S.; Alqahtani, R.; Rahman, M. Z.; Chang, B.; Gascon, J.; Zhang, H. B. Shining light on hydrogen: Solar-powered catalysis with transition metals. *Adv. Mater.* **2025**, *37*, 2410387.

[6] Yu, M. Y.; Ye, Q.; Wang, F.; Abdukayum, A.; Li, N. P.; Zhang, L.; Zuo, C.; Liu, W. P.; Zhao, X.; Hu, G. Z. Ternary metal NiRuPt partition synergistic relay promotes pH-universal hydrogen evolution. *Nano Res.* **2026**, *19*, 94907879.

[7] Xiao, L. Y.; Cheng, C. Q.; Yang, T. T.; Zhang, J. T.; Han, Y. J.; Han, C. Y.; Lv, W. X.; Tan, H. W.; Zhao, X. R.; Yin, P. F. et al. A "two-pronged" strategy to boost hydrogen evolution kinetics on NiFe-based (oxy)hydroxides via oxygen deficient Ni–Mo–Fe coordinate structures for ultra-stable ampere-level alkaline overall water splitting. *Adv. Mater.* **2024**, *36*, 2411134.

[8] Zhang, Y. J.; Nie, K. K.; Li, B. J.; Yi, L. X.; Hu, C.; Wang, Z. Y.; Hao, X. R.; Zhang, W. L.; Liu, Z. Q.; Huang, W. Cerium-optimized platinum-free high-entropy alloy nanoclusters for enhanced ampere-level sustainable hydrogen generation. *Appl. Catal. B: Environ. Energy* **2025**, *360*, 124529.

[9] Chen, D.; Bai, H. W.; Zhu, J. W.; Wu, C.; Zhao, H. Y.; Wu, D. L.; Jiao, J. X.; Ji, P. X.; Mu, S. C. Multiscale hierarchical structured NiCoP enabling ampere-level water splitting for multi-scenarios green energy-to-hydrogen systems. *Adv. Energy Mater.* **2023**, *13*, 2300499.

[10] Li, Y. J.; Sun, Y. J.; Qin, Y. N.; Zhang, W. Y.; Wang, L.; Luo, M. C.; Yang, H.; Guo, S. J. Recent advances on water-splitting electrocatalysis mediated by noble-metal-based nanostructured materials. *Adv. Energy Mater.* **2020**, *10*, 1903120.

[11] Hou, L. Q.; Li, Z. J.; Jang, H.; Wang, Y.; Cui, X. M.; Gu, X. M.; Kim, M. G.; Feng, L. G.; Liu, S. G.; Liu, X. E. Electronic and lattice engineering of ruthenium oxide towards highly active and stable water splitting. *Adv. Energy Mater.* **2023**, *13*, 2300177.

[12] Zhu, T.; Liu, S. H.; Huang, B.; Shao, Q.; Wang, M.; Li, F.; Tan, X. Y.; Pi, Y. C.; Weng, S. C.; Huang, B. L. et al. High-performance diluted nickel nanoclusters decorating ruthenium nanowires for pH-universal overall water splitting. *Energy Environ. Sci.* **2021**, *14*, 3194–3202.

[13] Wang, D. W.; Chen, Y. T.; Fan, L. B.; Xiao, T.; Meng, T.; Xing, Z. C.; Yang, X. R. Bulk and surface dual modification of nickel-cobalt spinel with ruthenium toward highly efficient overall water splitting. *Appl. Catal. B: Environ.* **2022**, *305*, 121081.

[14] Wang, Y.; Wang, S.; Ma, Z. L.; Yan, L. T.; Zhao, X. B.; Xue, Y. Y.; Huo, J. M.; Yuan, X.; Li, S. N.; Zhai, Q. G. Competitive coordination-oriented monodispersed ruthenium sites in conductive mof/ldh hetero-nanotree catalysts for efficient overall water splitting in alkaline media. *Adv. Mater.* **2022**, *34*, 2107488.

[15] Feidenhans'l, A. A.; Regmi, Y. N.; Wei, C.; Xia, D.; Kibsgaard, J.;

King, L. A. Precious metal free hydrogen evolution catalyst design and application. *Chem. Rev.* **2024**, *124*, 5617–5667.
[16] Jiang, J. Z.; Liu, S. G.; Li, Z. J.; Kim, M. G.; Jang, H.; Liu, X. E.; Hou, L. Q. Lattice-matched Ru/W_2C heterointerfaces with reversible hydrogen spillover for efficient alkaline hydrogen evolution. *Adv. Energy Mater.* **2025**, *15*, 2405546.
[17] Chen, S. Y.; Zhang, T.; Han, J. Y.; Qi, H.; Jiao, S. H.; Hou, C. M.; Guan, J. Q. Interface engineering of Fe–Sn–Co sulfide/oxyhydroxide heterostructural electrocatalyst for synergistic water splitting. *Nano Res. Energy* **2024**, *3*, e9120106.
[18] Wang, S. Y.; Zhang, L.; Li, X.; Li, C. L.; Zhang, R. J.; Zhang, Y. J.; Zhu, H. W. Sponge-like nickel phosphide-carbon nanotube hybrid electrodes for efficient hydrogen evolution over a wide pH range. *Nano Res.* **2017**, *10*, 415–425.
[19] Yang, M. Y.; Jiao, L.; Dong, H. L.; Zhou, L. J.; Teng, C. Q.; Yan, D. M.; Ye, T. N.; Chen, X. X.; Liu, Y.; Jiang, H. L. L. Conversion of bimetallic MOF to Ru-doped Cu electrocatalysts for efficient hydrogen evolution in alkaline media. *Sci. Bull.* **2021**, *66*, 257–264.
[20] Bai, H. W.; Chen, D.; Ma, Q. L.; Qin, R.; Xu, H. W.; Zhao, Y. F.; Chen, J. X.; Mu, S. C. Atom doping engineering of transition metal phosphides for hydrogen evolution reactions. *Electrochem. Energ. Rev.* **2022**, *5*, 24.
[21] Gao, Q. S.; Zhang, W. B.; Shi, Z. P.; Yang, L. C.; Tang, Y. Structural design and electronic modulation of transition-metal-carbide electrocatalysts toward efficient hydrogen evolution. *Adv. Mater.* **2019**, *31*, 1802880.
[22] Pu, Z. H.; Zhao, J. H.; Amiinu, I. S.; Li, W. Q.; Wang, M.; He, D. P.; Mu, S. C. A universal synthesis strategy for P-rich noble metal diphosphide-based electrocatalysts for the hydrogen evolution reaction. *Energy Environ. Sci.* **2019**, *12*, 952–957.
[23] Zheng, C. Y.; Zhang, X.; Zhou, Z.; Hu, Z. P. A first-principles study on the electrochemical reaction activity of 3d transition metal single-atom catalysts in nitrogen-doped graphene: Trends and hints. *eScience* **2022**, *2*, 219–226.
[24] Jiao, Y.; Zheng, Y.; Davey, K.; Qiao, S. Z. Activity origin and catalyst design principles for electrocatalytic hydrogen evolution on heteroatom-doped graphene. *Nature Energy* **2016**, *1*, 16130.
[25] Long, B.; Yang, H.; Li, M. Y.; Balogun, M. S.; Mai, W.; Ouyang, G. F.; Tong, Y. X.; Tsiakaras, P.; Song, S. Q. Interface charges redistribution enhanced monolithic etched copper foam-based Cu_2O layer/TiO_2 nanodots heterojunction with high hydrogen evolution electrocatalytic activity. *Appl. Catal. B: Environ.* **2019**, *243*, 365–372.
[26] Chen, J. X.; Fu, G. W.; Tian, Y. C.; Li, X. Q.; Luo, M. Q.; Wei, X. Y.; Zhang, T.; Gao, T.; Chen, C.; Chaemchuen, S. et al. Three-dimensional-printed Ni-based scaffold design accelerates bubble escape for ampere-level alkaline hydrogen evolution reaction. *Interdiscip. Mater.* **2024**, *3*, 595–606.
[27] Kempler, P. A.; Coridan, R. H.; Luo, L. Gas evolution in water electrolysis. *Chem. Rev.* **2024**, *124*, 10964–11007.
[28] Shen, P.; Zhou, B. W.; Chen, Z.; Xiao, W. P.; Fu, Y. L.; Wan, J.; Wu, Z. X.; Wang, L. Ruthenium-doped 3D Cu2O nanochains as efficient electrocatalyst towards hydrogen evolution and hydrazine oxidation. *Appl. Catal. B: Environ.* **2023**, *325*, 122305.
[29] Xi, W. S.; Jin, L. J.; Mahmood, A.; Zhang, W. K.; Li, Y. Y.; Li, H.; An, P. F.; Zhang, J.; Ma, T. Y.; Liu, S. et al. Accelerating Ru^0/Ru^{4+} adjacent dual sites construction by copper switch for efficient alkaline hydrogen evolution. *Adv. Energy Mater.* **2023**, *13*, 2302668.
[30] Tensile strain and low coordination activate pure copper for hydrogen evolution. *Nat. Mater.* **2025**, *24*, 342–343.
[31] Hausmann, J. N.; Schlögl, R.; Menezes, P. W.; Driess, M. Is direct seawater splitting economically meaningful. *Energy Environ. Sci.* **2021**, *14*, 3679–3685.
[32] Liang, J.; Li, Z. X.; He, X.; Luo, Y. S.; Zheng, D. D.; Wang, Y.; Li, T. S.; Ying, B. W.; Sun, S. J.; Cai, Z. W. et al. Electrocatalytic seawater splitting: Nice designs, advanced strategies, challenges and perspectives. *Mater. Today* **2023**, *69*, 193–235.
[33] Shen, L. W.; Wang, Y.; Shen, L.; Chen, J. B.; Liu, Y.; Hu, M. X.; Zhao, W. Y.; Xiong, K. Y.; Wu, S. M.; Lu, Y. et al. Ruthenium nanoparticles decorated with surface hydroxyl and borate species boost overall seawater splitting via increased hydrophilicity. *Energy Environ. Sci.* **2024**, *17*, 3888–3897.
[34] Xiao, M. J.; Wu, C.; Zhu, J. W.; Zhang, C. T.; Li, Y.; Lyu, J. H.; Zeng, W. H.; Li, H. W.; Chen, L.; Mu, S. C. *In situ* generated layered NiFe-LDH/MOF heterostructure nanosheet arrays with abundant defects for efficient alkaline and seawater oxidation. *Nano Res.* **2023**, *16*, 8945–8952.
[35] Shi, G. Y.; Tano, T.; Tryk, D. A.; Yamaguchi, M.; Iiyama, A.; Uchida, M.; Iida, K.; Arata, C.; Watanabe, S.; Kakinuma, K. Temperature dependence of oxygen evolution reaction activity in alkaline solution at Ni–Co oxide catalysts with amorphous/crystalline surfaces. *ACS Catal.* **2022**, *12*, 14209–14219.
[36] Yue, C. Z.; Zheng, W. B.; Wang, Q. Y.; Wang, Z. D.; Li, B.; Zhang, C. M.; Ming, P. W. Challenges in membrane electrode assemblies at elevated temperatures for proton exchange membrane fuel cells: A review. *Energy Environ. Sci.* **2025**, *18*, 6934–6982.
[37] Hyun Oh, J.; Ho Han, G.; Kim, J.; Eun Lee, J.; Kim, H.; Kyung Kang, S.; Kim, H.; Wooh, S.; Soo Lee, P.; Won Jang, H. et al. Self-supported electrodes to enhance mass transfer for high-performance anion exchange membrane water electrolyzer. *Chem. Eng. J.* **2023**, *460*, 141727.
[38] Zhu, S. Q.; Qin, X. P.; Xiao, F.; Yang, S. L.; Xu, Y.; Tan, Z.; Li, J. D.; Yan, J. W.; Chen, Q.; Chen, M. S. et al. The role of ruthenium in improving the kinetics of hydrogen oxidation and evolution reactions of platinum. *Nat. Catal.* **2021**, *4*, 711–718.
[39] Zhu, C. Y.; Ye, Q.; Li, C. Y.; Wang, F.; Yu, M. Y.; Abdukayum, A.; Zuo, C.; Liu, W. P.; Hu, G. Z.; Zhao, X. Morphology-induced surface growth of random nano-ruthenium promotes the hydrogen evolution reaction. *Chem. Commun.* **2025**, *61*, 19120–19123.
[40] Wang, Y. H.; Zheng, S. S.; Yang, W. M.; Zhou, R. Y.; He, Q. F.; Radjenovic, P.; Dong, J. C.; Li, S. N.; Zheng, J. X.; Yang, Z. L. et al. *In situ* Raman spectroscopy reveals the structure and dissociation of interfacial water. *Nature* **2021**, *600*, 81–85.
[41] Zhao, X.; Jiang, Y. L.; Wang, D.; Zhang, Y. C.; Chen, M. S.; Hu, G. Z.; Zhang, H. B.; Jin, Z.; Zhou, Y. T. PtRu intra-cluster electron modulation accelerates multi-scenario hydrogen evolution reaction. *Adv. Energy Mater.* **2025**, *15*, 2405828.